Impulse Generation by an Open Shock Tube

J. Kasahara*
University of Tsukuba, Tsukuba 305-8573, Japan
and
Z. Liang,[†] S. T. Browne,[‡] and J. E. Shepherd[§]
California Institute of Technology, Pasadena, California 91125

We perform experimental and numerical studies of a shock tube with an open end. The purpose is to investigate the impulse due to the exhaust of gases through the open end of the tube as a model for a partially filled detonation tube as used in pulse detonation engine testing. We study the effects of the pressure ratio (varied from 3 to 9.2) and the volume ratio (expressed as fill fractions) between the driver and driven section. Two different driver gases, helium and nitrogen, and fill fractions between 5 and 100% are studied; the driven section is filled with air. For both driver gases, increasing the pressure ratio leads to larger specific impulses. The specific impulse increases for a decreasing fill fraction for the helium driver, but the impulse is almost independent of the fill fraction for the nitrogen driver. Two-dimensional (axisymmetric) numerical simulations are carried out for both driver gases. The simulation results show reasonable agreement with experimental measurements at high pressure ratios or small fill fractions, but there are substantial discrepancies for the smallest pressure ratios studied. Empirical models for the impulse in the limits of large and small fill fractions are also compared with the data. Reasonable agreement is found for the trends with fill fractions using the Gurney or Sato model at large fill fractions, but only Cooper's bubble model is able to predict the small fill fraction limit. Computations of acoustic impedance and numerical simulations of unsteady gas dynamics indicate that the interaction of waves with the driver-driven gas interface and the propagation of waves in the driven gas play an essential role in the partial-fill effect.

Introduction

MOTIVATED by recent interest in pulse detonation engines [1], a number of researchers [2–12] have studied the impulse from a partially filled detonation tube. In these experiments and analyses, a portion of the detonation tube near the closed end (thrust surface) contains the combustible mixture whereas the remaining portion of the tube up to the open end contains an inert gas mixture, for example, air. The general conclusion of these studies is that an inert section will increase the specific impulse (impulse per unit mass of combustible mixture) although the total impulse decreases. Based on these studies, the use of partially filled detonation tubes has been proposed as a technique for improving a specific performance. A number of simple models have been proposed to account for the partial-fill effect but there is no consensus regarding the best way to model this effect and correlate performance. Comparisons between experiments and models only cover a limited range of fill fractions, which prevents crucial tests of the models. It is not possible to generate an ideal detonation in an extremely short tube section and, if sufficiently long detonation sections are used, the inert portion of the tube would be of an impracticable length for the smallest fill fractions of interest. In addition, nonideal processes such as heat transfer losses may be significant [13,14] in detonation tubes.

To better understand the physical mechanisms behind the partial-fill enhancement of a specific performance, we are motivated to examine the simpler case of a shock tube with an open end. Experimentally, we can more readily vary the parameters, including the fill fraction and the initial pressure ratio, than is possible in

detonation experiments. Numerically, the nonreacting gas dynamics of the shock tube can be accurately simulated using the perfect gas models for the driver and driven section. We can examine the limiting value of a specific impulse as the fill fraction approaches zero and compare the results with models proposed for this case. Cooper [6] predicted that the specific impulse will approach a limiting value on the basis of a simple model, but it is experimentally difficult to approach this limit in the detonation case. Other approximate models [5,8,11–13] have also been proposed to predict the specific impulse dependence on the fill fraction when the fill fraction is close to 1. We examine both limits experimentally, carry out detailed numerical simulations, and compare the results to the approximate analytical models.

The design of our experiments is motivated by the simulations of Li and Kailasanath [8] and considerations of the fundamental gas dynamic processes associated with wave propagation in shock and detonation tubes. Their simulations showed that the main differences between partially and fully filled tubes can be understood by focusing on the interaction of the detonation and expansion waves with the interface between the fueled and inert sections, in addition to the reflection of the waves at the open end of the tube. The pressure history at the ignition (closed) end of the detonation tube is controlled by the arrival time of the expansion waves generated by these interactions and the subsequent rate of pressure decay. The increase in specific impulse associated with partial filling is shown to be a consequence of the lower rate of decay associated with the weaker expansion waves from the detonation interaction with the interface as compared with the interaction with the open end of the tube. The wave interaction processes at the interface between the fueled and inert sections is determined for weak waves [15] by the ratio of acoustic impedances (the product of density ρ and sound speed a) for the states on each side of the interface. In the case of detonation tubes, this ratio can be computed [16] by using one-dimensional wave interaction diagrams [15] to find the state of the gas on each side of the interface immediately after the detonation passes through the interface.

The initial interaction of the detonation wave with the interface results in a transmitted shock and reflected expansion in almost all cases [16]. For example, in the case of a detonation propagating in a

*Associate Professor.
†Postdoctoral Scholar, Aeronautics.
‡Graduate Student, Aeronautics.
§Professor, Aeronautics.

stoichiometric ethylene-oxygen section (initial state $1'$) bounded by air (initial state 1), a shock of Mach number 4.73 is transmitted into the air (postshock state 2). An expansion wave (pressure decrease of 0.63 MPa) propagates back into the detonation products at Chapman–Jouguet state, creating a state $2'$ in the detonation products next to the interface (see the $x–t$ diagram of Fig. 1). Numerical computation [17] using realistic thermochemistry gives the result that the ratio of acoustic impedance across interface just following the wave interaction is $(\rho a)_2/(\rho a)_{2'} = 1.96$. With flow out of the detonation tube, the products depressurize in a nearly isentropic manner [16], which results in the density and sound speed on both sides of the interface decreasing as the pressure drops. Numerical computation reveals that the ratio of acoustic impedance across the interface is practically independent of the pressure, and so we can take the ratio to be approximately constant (≈ 2) throughout the pulse detonation tube cycle of operation. Although the detonation products are hotter than the shocked air, the detonation products have a smaller density, and so the acoustic impedance of the shocked air is higher than the detonation products' acoustic impedance. An acoustic wave originating in the detonation products and incident on the interface $2'–2$ will reflect with an increase of amplitude [15] of approximately $4/3$ and, when those waves subsequently reflect from the end wall, the amplitude will double. This leads to the trapping of acoustic waves between the end wall and the interface, which we believe is a key physical process in the partial-fill effect.

In an ideal shock-tube operation, Fig. 2, a contact surface is created by the rupture of the diaphragm separating state 4 (driver gas) from state 1 (driven section gas). The analog of the interface $2'–2$ in the detonation case is the contact surface 2–3, which separates the driven section gas that has been shocked (state 2) and the driver section gas that has been expanded (state 3) The impedance ratio $(\rho a)_2/(\rho a)_3$ will be a function of the properties (molar mass and specific heat ratio) of both the driver and driven gases as well as the operating conditions of the shock tube P_4/P_1 and T_4/T_1. To examine the influence of the impedance ratio on impulse generation, we carry out shock-tube experiments and simulations with two sets of driver and

Table 1   Shock-tube solutions, states, and interface impedance ratios; all gases are initially at 295 K and the air is at 100 kPa

P_4/P_1	M_s	P_2/P_1	T_2/T_1	T_3/T_4	$(\rho a)_2/(\rho a)_3$
	He driver and air driven section				
1.0	1.0	1.0	1.0	1.0	2.468
3.0	1.405	2.14	1.26	0.863	2.025
6.0	1.74	3.35	1.49	0.771	1.737
9.2	1.971	4.37	1.66	0.714	1.565
	N_2 driver and air driven section				
1.0	1.0	1.0	1.0	1.0	1.018
3.0	1.265	1.70	1.17	0.837	0.851
6.0	1.460	2.32	1.29	0.731	0.742
9.2	1.589	2.78	1.38	0.667	0.667

driven gas combinations. By using a helium driver and an air driven section, we can produce acoustic impedance ratios at the helium/air interface that are very similar to those obtained in the detonation case (see Table 1). On the other hand, by using a nitrogen driver and an air driven section, the impedance ratio is slightly less than one (see Table 1) When the acoustic impedance ratio is unity, acoustic disturbances pass through the interface unmodified in amplitude, and no reflected waves are created. Therefore, in the case of a nitrogen driver, we can essentially eliminate all wave interaction effects at the driver/driven gas interface. By comparing the He and N_2 driver cases, we can discriminate between the effect of the acoustic impedance ratio (wave trapping) and the inertial confinement. If the partial-fill effect is primarily associated with wave trapping, the helium and nitrogen drivers should show dramatically different results as a function of the fill fraction. On the other hand, if the partial-fill effect is primarily due to inertial confinement, then we expect to observe much less difference in the two cases.

Experiments

As shown in Fig. 3, the experimental apparatus is a partially filled shock tube. This conventional shock tube consists of a cylindrical driver of fixed length (101 mm) to which cylindrical extensions (the driven section) of various lengths (12.7–1814 mm) are added. The driver section is filled with pressurized gas (helium or nitrogen) and initially sealed by a thin polyethylene-terephthalate plastic diaphragm separating the driver and driven section. The driven section is open to the atmosphere. The initial conditions in the driven section matched those of the room, nominally 22°C and $P_a = 1$ atm. In the driver section, the initial temperature is also room temperature, but the initial pressure is varied from $P_0/P_a = 9.2$ to 2.0.

To start the experiment, the diaphragm is ruptured using a pneumatically activated cutter. A cutter is used to minimize the diaphragm rupture time, to make the opening process as ideal as possible, and to ensure that the rupture took place at specified and reproducible driver pressures. The pressurized driver gas expands into the driven section, creating a shock in the driven section that propagates to the open end of the driven section and diffracts into the surrounding atmosphere. This resulting wave system, illustrated in Fig. 4, is similar to that observed in detonation tube experiments and models [13,16]. An expansion wave (E_1), centered at the initial location of the diaphragm, propagates toward the thrust surface, the closed end wall of the driver section. Initially, the pressure on the closed end surface is equal to the initial pressure of the driver P_0 and remains constant in the interval $t_0–t_1$. During the initial reflection of the expansion wave, the pressure decreases during the time interval $t_1–t_2$ and remains constant again during the interval $t_2–t_3$. After sufficient time has elapsed, 3–4 ms, the pressure inside the tube reaches the ambient value P_a. As shown in Fig. 5, the impulse is measured mechanically using the ballistic pendulum apparatus detailed in Cooper et al. [18], and the pressure history on the closed end is measured with a piezoelectric pressure transducer. The partially filled shock tube is suspended by four stainless-steel wires from the ceiling of the experimental room. The effective wire length of the pendulum (ℓ) is 1987 mm. The maximum displacement of the
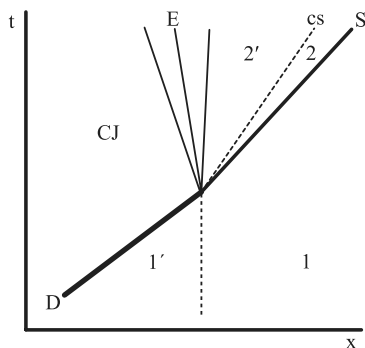

Fig. 1   Interaction of a detonation wave (D) with a contact surface (cs) creating a shock (S) and an expansion (E) wave.
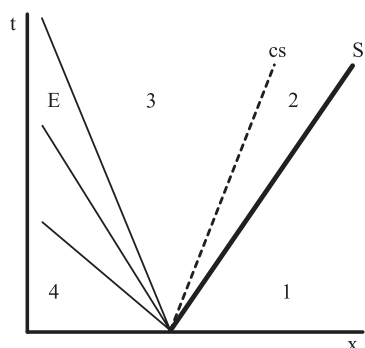

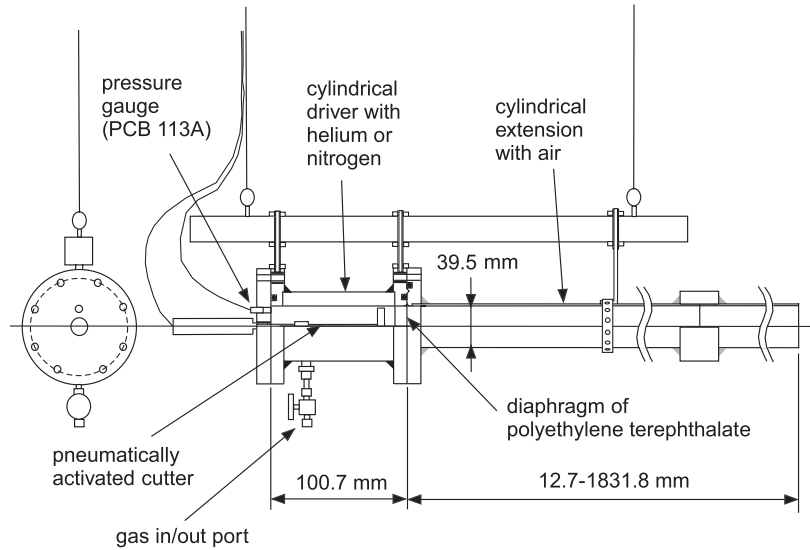**Fig. 2   Ideal shock-tube operation creating a shock wave (S), contact surface (cs), and expansion (E) wave.**

Fig. 3 Partially filled shock tube consisting of a cylindrical driver and cylindrical extensions.
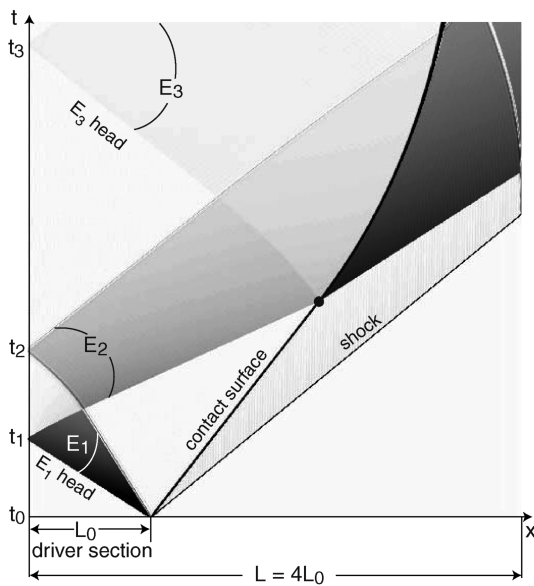

Fig. 4 x–t diagram of inert gas dynamics in a partially filled shock tube. E_1, E_2, and E_3 represent the three expansion fans discussed in the text.

shock tube in the horizontal direction (x_m) is measured by using a video camera. When $\ell \gg x_m$, the impulse I is given by elementary mechanics to be

$$I = Mx_m\sqrt{\frac{g}{\ell}} \qquad (1)$$

where M is the mass of the partially filled shock tube, and g is the gravitational acceleration. The specific impulse is

$$I_{sp} = \frac{I}{m_0 g} = \frac{Mx_m}{\rho_0 V_0}\sqrt{\frac{1}{g\ell}} \qquad (2)$$

where m_0, ρ_0, and V_0 are the mass, initial density, and initial volume of the driver gas (helium or nitrogen), respectively.

Numerical Model

The computational domain is shown in Fig. 6. Because the geometry is symmetric, only half of the domain is computed. The tube diameter, $d = 39.5$ mm, and driver section length, $L_0 = 101$ mm, are constant. The driven section varies between 0 and 1.84 m. The fill fraction, α, is defined as $\alpha = L_0/L$, where L is the total shock-tube length. The total computational domain size is
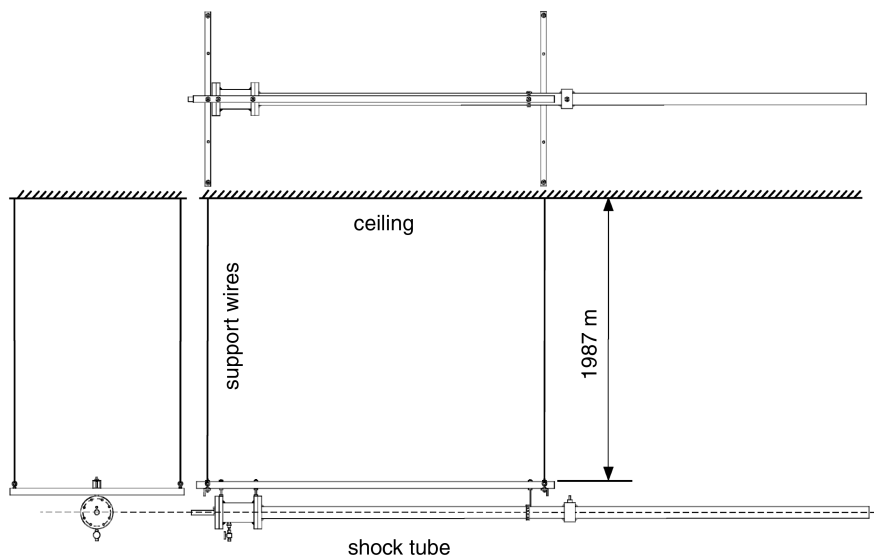

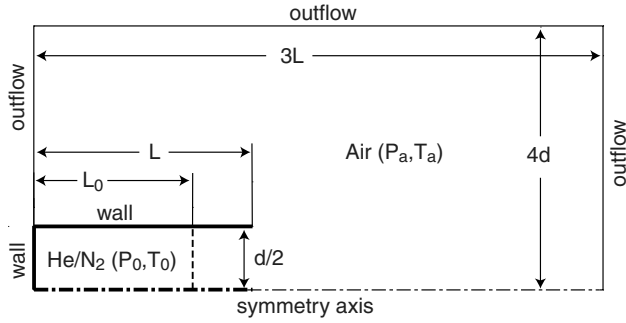Fig. 5 Experimental setup of the partially filled shock tube.

Fig. 6 Geometry and gas regions used in the computational model. $L_0 = 101$ mm, $L = 0$–1.84 m, $d = 39.5$ mm, $P_a = 1$ atm, $T_a = 295$ K, $P_0/P_a = 3.0$–9.2, and $T_0 = 295$ K.

$3L$ (length) by $4d$ (width). An outflow boundary condition is implemented on the top, left (except at the closed end of the shock tube), and right sides. The bottom side is the symmetry boundary. The corresponding gas parameters are listed in Table 2.

The problem is modeled using the two-dimensional (axisymmetric), inviscid, nonreactive Euler equations with the perfect gas equation of state. For the temperature range of interest for the present tests, the gases can be adequately represented by a constant heat capacity computed from the appropriate ratio of specific heats, γ_1 and γ_2, for the driver and driven gases.

$$c_{p_i} = (\gamma_i R)/(\gamma_i - 1) \tag{3}$$

The specific heat for the mixture is then given by

$$c_p = \sum_{i=1,2} Y_i c_{p_i} \tag{4}$$

where Y_i is the mass fraction of the gases. Away from the interface region where some numerical diffusion takes place, the mass fractions are either one or zero. The details of the implementation of the mixture model are given in Deiterding [19].

The equations are solved with an explicit second-order Godunov-type numerical scheme incorporating a hybrid Roe-solver-based method. A block-structured adaptive mesh refinement technique is used to supply the required resolution locally [20]. This adaptive method uses a hierarchy of spatially refined subgrids that are integrated recursively with reduced time steps.

In the numerical simulations, the impulse is computed by first finding the spatial average of the pressure on the closed end to determine the net force on the tube as a function of time. The force is then numerically integrated in time to find the total impulse:

$$I = \int F \, dt = \int_0^{t_{\text{final}}} (P(t) - P_a) A_0 \, dt \tag{5}$$

where $P(t)$ is the spatial average of the pressure on the thrust surface, P_a is the ambient pressure, A_0 is the cross-sectional area of the driver section, and t_{final} is the final time reached in the simulation. The simulation is carried out until $P(t)$ is reasonably close to P_a. The trapezoidal rule is used to perform the integration and, in the current computations, $t_{\text{final}} = 4$ ms for helium and $t_{\text{final}} = 8$ ms for nitrogen.

The specific impulse based on the total driver mixture mass is defined as

$$I_{\text{sp}} = \frac{I}{\rho_0 V_0 g} = \int_0^{t_{\text{final}}} \frac{(P(t) - P_a)}{\rho_0 L_0 g} \, dt \tag{6}$$

Table 2 Gas parameters

Gas	γ	W, g/mol	ρ at 1 atm, kg/m³
He	1.66	4.0	0.1787
N$_2$	1.406	28.0	1.2506
Air	1.40	29.0	1.2250

Approximate Models

A number of approximate models have been proposed for correlating the impulse with the fill fraction and the thermodynamic properties of the mixture. We have examined three of these in the present study: the Gurney model [21] based on energy conservation, a "bubble" model based on acoustic analysis, and an empirical model by Sato et al. [11]. The Gurney and Sato models are useful for large fill fractions, whereas the bubble model is designed to deal with the limiting case of a very small fill fraction.

Gurney Model

The Gurney model was originally developed to predict the acceleration of metal by the detonation of explosives [21,22]. The model is based on energy conservation and a simple approximation of the velocity in the detonation products. The Gurney model for explosives suggests a simple approach for predicting the value of the impulse for pulse detonation tubes [5,6] and can be extended to the present case by analogy. The results of the Gurney model can be expressed in terms of the mass M of the shock tube, the mass C of the pressurized driver gas, and the mass N of the air in the driven section, which is referred to as the "tamping" mass in the case of explosives. The impulse predicted [5] by the Gurney model is

$$I = M\sqrt{2e}\left(\sqrt{\frac{1 + A^3}{3(1 + A)} + A^2 \frac{N}{C} + \frac{M}{C}}\right)^{-1} \tag{7}$$

where

$$A = (1 + 2\tfrac{M}{C})/(1 + 2\tfrac{N}{C}) \tag{8}$$

and e is the Gurney energy of the explosive, in this case, the pressurized driver gas. The Gurney energy is taken to be a percentage of the ideal amount of specific energy available to do mechanical work:

$$e = \eta e_i \tag{9}$$

where η is the empirically determined energy efficiency (see the subsequent section entitled Energy Efficiency). Assuming the isentropic expansion of the pressurized gas,

$$e_i = \frac{P_0}{(\gamma - 1)\rho_0}\left[1 - \left(\frac{P_0}{P_a}\right)^{1/\gamma - 1}\right] \tag{10}$$

Typically, $M/C \to \infty$, and we can rewrite Eq. (7) in term of the specific impulse:

$$I_{\text{sp}} = \frac{I}{Cg} = \frac{\sqrt{2e}}{g}\frac{\frac{N}{C} + \frac{1}{2}}{\sqrt{\frac{N}{C} + \frac{1}{3}}} \tag{11}$$

The mass of the pressurized gas C and the mass of the air N can be related to the partial-fill fraction α:

$$\alpha = \left(\frac{C}{\rho_0}\right)/\left(\frac{C}{\rho_0} + \frac{N}{\rho_a}\right) = 1/\left(1 + \frac{\rho_0}{\rho_a}\frac{N}{C}\right) \tag{12}$$

where ρ_a is the density of the air and ρ_0 is the initial density of the driver gas.

For a fully filled tube, that is, without any tamping gas ($N = 0$), $\alpha = 1.0$, and the specific impulse $I_{\text{sp}}(\alpha = 1)$ is

$$I_{\text{sp}}(\alpha = 1) = \sqrt{1.5e}/g \tag{13}$$

Then the ratio of $I_{\text{sp}}/I_{\text{sp}}(\alpha = 1)$ is

$$\frac{I_{\text{sp}}}{I_{\text{sp}}(\alpha = 1)} = \sqrt{\frac{4}{3}}\frac{\frac{N}{C} + \frac{1}{2}}{\sqrt{\frac{N}{C} + \frac{1}{3}}} \tag{14}$$

which only depends on the ratio of N/C.

Table 3 Specific impulse $I_{sp}(\alpha = 1)$ computed from the Gurney model, assuming an energy efficiency of $\eta = 30\%$

Gas	P_0/P_a	e_i, MJ/kg	$I_{sp}(\alpha = 1)$, s
He	3.0	0.509	48.83
	6.0	0.965	67.25
	9.2	1.333	79.04
N_2	3.0	0.081	19.42
	6.0	0.146	26.17
	9.2	0.196	30.30

Table 3 shows the specific impulse $I_{sp}(\alpha = 1)$ computed with Eq. (11). For explosives, the Gurney energy is some fraction of the heat of combustion of the explosive, and we expect in the present case that it will be some fixed fraction η of the ideal energy given by Eq. (10). For detonation tubes, a value of $\eta = 0.3$ was determined [5,6]. For the present case, we have determined the efficiency by fitting the Gurney model results to either the experimental data or the computation results with a least-squares method.

The Gurney model is clearly dependent only on the mass ratios of the driver and driven gas for a given value of the Gurney energy. Acoustic impedance and other properties of the gases do not enter into the result. If inertia plays the dominant role in the partial-fill effect and the Gurney model is valid, then we would expect to have the same qualitative behavior for both the N_2 and He drivers, and the quantitative differences will be predicted by the scaling with mass ratio as in Eq. (11). We will test this against the experimental data in the Results section.

Bubble Model

The expanding bubble model of detonation hot products [6] predicts the specific impulse in the limit of $\alpha \to 0$. It is useful because, unlike the Gurney model, the bubble model predicts a finite value of specific impulse in the limiting case of a small α, and the numerical value is consistent [6] with the available experimental data. Here we use the same idea to analyze the shock tube. The essential notions are that 1) the acoustic transit time across the driver is small in comparison to the duration of the interface motion, and 2) the reverberation of the acoustic waves inside the driver creates an approximately spatially uniform condition that can be modeled as isentropic expansion. Although the acoustic impedance ratio does not appear explicitly in the model, it is essential to have the trapping of acoustic waves in the driver region to create the bubble of driver gas that is isentropically expanding. The acoustic impedance in the driver gas does explicitly enter the model and links the interface speed to the pressure in the bubble, which is also an essential ingredient in the bubble model. The bubble model relies on wave motion to determine the dynamics rather than the energy and inertia considerations of the Gurney model.

Assuming that the pressurized driver gas expands isentropically and there is no significant spatial variations within the driver gas, the change in pressure, $P(t)$, can be related to the length of the driver as a function of time:

$$P(t) = P_0\left(L_0/x(t)\right)^{\gamma_0} \tag{15}$$

where $x(t)$ is the location of the contact surface that separates the driver and driven gas in an ideal one-dimensional shock-tube model. The idea behind the bubble model is that the contact surface velocity induces a flow and pressure drop in the driver gas. This flow can be computed using the method of characteristics or using acoustic theory in a linearized version for small velocities. This yields [6] an ordinary differential equation for the contact surface velocity:

$$\frac{dx}{dt} = \frac{2c_o}{\gamma_a - 1}\left(\frac{x}{L_0}\right)^{\frac{\gamma_o}{2\gamma_a}(1-\gamma_a)}\left(\frac{P_0}{P_a}\right)^{\frac{1}{2\gamma_a}(\gamma_a-1)-1} \tag{16}$$

where γ_o and γ_a represent the specific heat ratio of the driver gas and the air. Equation (16) can be numerically integrated until the contact surface reaches the final position. Time integration of the pressure history at the closed end yields the predicted impulse. Figure 7a shows an x–t diagram of the contact surface trajectories for several cases. The pressure histories for several pressure ratios are plotted in Fig. 7b. The pressure decays faster for higher initial pressure ratios and larger specific heat ratios, γ, in the driver gas.

Table 4 lists the specific impulse in the limit of $\alpha \to 0$ or $L \to \infty$, $I_{sp}(\alpha \to 0)$, computed with Eq. (16) for each driver case. Note the dramatic differences in the values predicted for He and N_2; this will provide a very clear-cut test when compared against the experimental data.

Sato Model

Sato et al. [11] proposed a simple empirical formula for predicting $I_{sp}/I_{sp}(\alpha = 1)$:

$$I_{sp}/I_{sp}(\alpha = 1) = 1/\sqrt{Z} \tag{17}$$

where Z is related to the fill fraction α by

$$Z = \alpha\rho_0/(\alpha\rho_0 + (1-\alpha)\rho_a) \tag{18}$$

Z can also be related to the mass ratio of N/C by substituting Eq. (12) into Eq. (18):

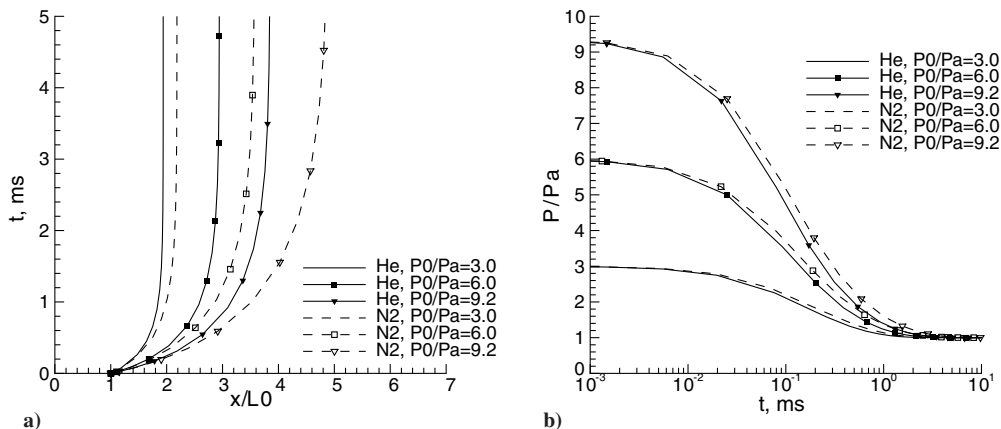$$Z = 1/(1 + N/C) \tag{19}$$

Now Eq. (17) becomes

Fig. 7 Results of the numerical integration of the bubble model, Eq. (16): a) x–t diagram illustrating contact surface trajectory, and b) pressure histories illustrating pressure decay as a function of time for the three initial pressure ratios and the two driver gases.

Table 4　Specific impulse $I_{sp}(\alpha \to 0)$ computed with the bubble model

Gas	P_0/P_a	$I_{sp}(\alpha \to 0)$, s
He	3.0	105.04
	6.0	124.97
	9.2	128.57
N_2	3.0	18.79
	6.0	23.26
	9.2	24.61

$$\frac{I_{sp}}{I_{sp}(\alpha = 1)} = \sqrt{1 + \frac{N}{C}} \qquad (20)$$

Like the Gurney model, the Sato model only depends on the inertia of the driver and driven gases. The Sato model shares the defect of the Gurney model of predicting an infinite specific impulse in the limit of zero fill fraction. This is also true of the homogeneous dilution model recently put forward by Endo et al. [12]

Simulation and Experimental Results

Pressure and Impulse History

Figure 8 shows the simulation results of the average pressure time histories on the thrust surface and the specific impulse for two fill fractions with helium as the driver gas. The time t_1 (Fig. 4) is defined by the head of the expansion fan (E_1) reaching the thrust surface. Because the length of the driver is fixed, t_1 is only a function of the driver gas conditions. This is because the speed of the expansion fan is determined by the sound speed in the driver gas. The sound speed in helium is 1008 m/s, and so t_1 is ≈ 0.1 ms. For the maximum fill fraction, $\alpha = 1.0$ (Fig. 8a), the pressure on the thrust surface, $P(t)$, decays below the ambient pressure P_a at between 0.1 and 0.12 ms depending on the pressure ratio. Then it begins to oscillate, but all oscillations are damped out by 4 ms for all pressure ratios. In each case, the specific impulse reaches its maximum value when $P(t) = P_a$ and then decreases to its minimum value due to the negative impulse generated when $P(t) < P_a$. For higher pressure ratios, the ratio of the final average specific impulse $\bar{I}_{sp}$ to the maximum specific impulse $I_{sp,max}$ is close to 1, but in the low pressure ratio case ($P_0/P_a = 3$), $\bar{I}_{sp}/I_{sp,max}$ is almost 0.7. The same features in the pressure signals were observed in the experiments, shown in Fig. 9. In the experiments, $t = 0$ corresponds to when the data acquisition system was triggered, and the negative time period ($t < 0$) represents the pretrigger signals. The impulse values were not computed from the pressure signals because we cannot assign a time to the onset of diaphragm rupture.

In the computations, before $P(t)$ decays below P_a in the lower fill fraction case, $\alpha = 0.6$ (Fig. 8b), there exists a second plateau. In this
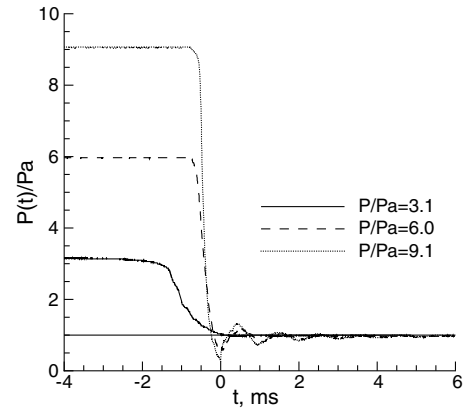
Fig. 9　Experimental pressure profile at the thrust wall vs time for $\alpha = 0.89$ in He/air.

case, the expansion wave (E_3) (Fig. 4), which is radiating toward the thrust surface from the interaction of the reflected expansion fan (E_2) and the contact surface, must travel farther as the length of the driven section is longer. The reflection of the expansion waves and the second plateau region are also observed in the simulations of Li and Kailasanath [8] and Endo et al. [12]. In the $\alpha = 0.6$ case, E_3 reaches the thrust surface later than in the $\alpha = 1.0$ case. Hence, the specific impulse is larger than the $\alpha = 1.0$ case at the same pressure ratio. The pressure oscillations are also damped more quickly than in the $\alpha = 1.0$ case.

The pressure and specific impulse histories for nitrogen are shown in Fig. 10. Because the sound speed in nitrogen (350 m/s) is lower than in helium, the initial pressure starts decreasing at a later time, $t_1 \approx 0.29$ ms. The second constant-pressure stage in nitrogen starts when the pressure has dropped below the atmospheric pressure. The specific impulse reaches a maximum before this second stage starts; therefore, the final specific impulse for nitrogen is smaller than for helium at the same fill fraction. For smaller fill fractions, the second constant-pressure stage lasts longer, so that the specific impulse has a larger decrease, that is, $I_{sp} \approx 20$ s at $t = 1$ ms for $P_0/P_a = 3$ and drops down to ≈ 8 s at 4 ms. For this reason, longer integration time periods are necessary for nitrogen mixtures at lower fill fractions.

We observe that the helium and nitrogen cases are fundamentally different due to the wave interaction processes at the contact surface. The reflection of the expansion wave in the helium case leads to the development of the second pressure plateau in the driver end wall pressure history, whereas in the nitrogen case no reflection occurs and the second plateau does not exist. This can be clearly observed by comparing the space–time diagrams for the case of a helium driver, Fig. 11a, and a nitrogen driver, Fig. 11b, both for $\alpha = 0.1$. A distinct sequence of reflected and transmitted expansion waves can be observed in the helium case and the air–helium interface is quickly

a)

b)
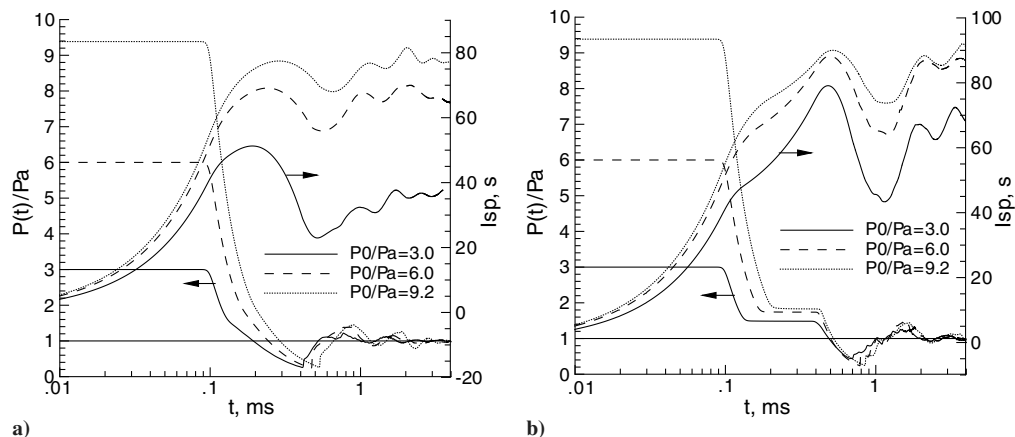
Fig. 8　Results of the numerical simulation for the normalized pressure and specific impulse vs time in He/air: a) $\alpha = 1.0$, and b) $\alpha = 0.6$.
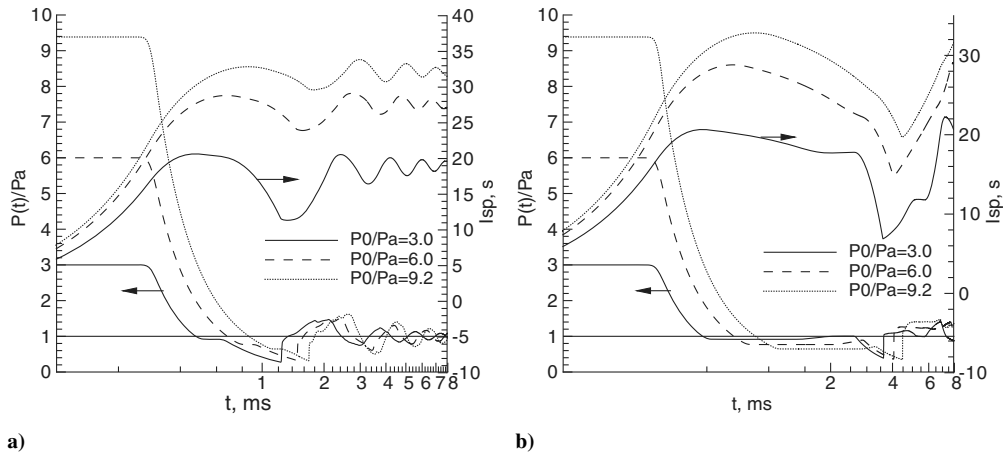
Fig. 10 Results of the numerical simulation for the normalized pressure and specific impulse vs time in N_2/air: a) $\alpha = 0.8$, b) $\alpha = 0.2$.
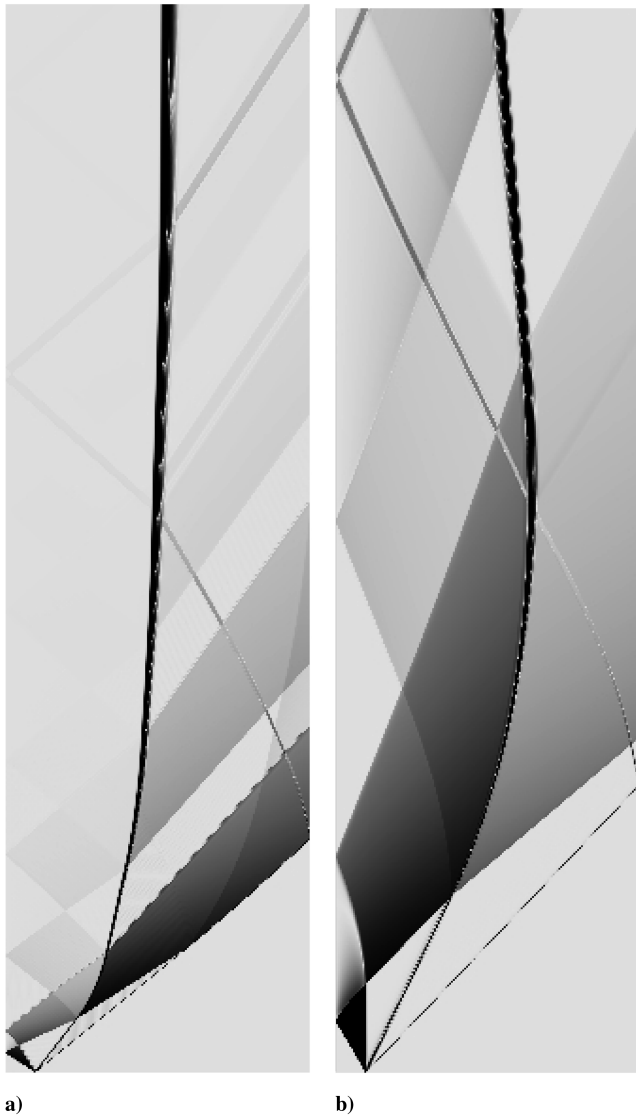

a)   b)

Fig. 11 Computed space–time diagrams (the gray scale simulates a schlieren effect) showing the wave processes for the two cases, both with $\alpha = 0.1$ and $P_4/P_1 = 10$: a) He driver, b) N_2 driver.

brought to a stop, whereas much weaker reflected waves are observed in the nitrogen case and the interface expands to a much larger distance, then rebounds. The second pressure plateau results in a higher specific impulse for the helium case compared with the

nitrogen case. This points directly to the strong role of the impedance ratio at the interface and the wave interaction processes in the partial-fill effect.

Specific Impulse

The specific impulse computed from the numerical simulations, analytical models, and experimental measurements are compared in Figs. 12–15.

Effect of Fill Fraction

The general trend shown in Figs. 12–14 is the same for all of the pressure ratios examined. For helium, the I_{sp} increases as α decreases until $\alpha < 0.2$, at which point the I_{sp} reaches a maximum value. For nitrogen, the I_{sp} remains almost constant and independent of α over the entire range of values examined. No partial-fill enhancement effect is observed for the nitrogen driver, and a very strong partial-fill effect is observed with the helium driver. This is consistent with our conjecture about the role of the acoustic impedance ratio at the driver-air interface and the values given in Table 1. The range of driven-to-driver mass ratios (N/C) in Eq. (12) is a factor of 7 smaller for the nitrogen driver rather than the helium due to the molecular weight difference. However, just comparing the same range of N/C values, it is quite clear that the qualitative behavior of the impulse as a function of α is fundamentally different for helium than for nitrogen.

As expected, the Gurney and bubble models are useful only over restricted ranges of the fill fraction. For small fill fractions, $\alpha < 0.2$, the bubble model shows reasonable agreement with experiments and simulations for both gases. The disagreement between the model and the data is largest for the lower pressure ratio $P_0/P_a = 3.0$. In the limit of zero fill fraction, the bubble model gives finite specific impulse values that are consistent with the experiments, whereas the Gurney model predicts totally unrealistic values that diverge to infinity as $\alpha \rightarrow 0$. This is sensible because the dynamics must be determined by wave propagation when the driven section becomes sufficiently long compared with the driver. For larger fill fractions, $\alpha > 0.3$, the Gurney model has the same trends as the experiments and simulations for helium. It is possible to obtain quantitative agreement only over a limited range of α by selecting a particular value of energy efficiency, but there is no universal value for this parameter that matches all of the data. The partial agreement of the Gurney model for helium is clearly fortuitous and the disagreement with the nitrogen data rules out a mass-ratio based (inertial) model of the partial-fill effect.

The simulation and experimental results are in reasonable agreement (within 20%) for the two higher pressure ratios, $P_0/P_a = 9.2$ and 6.0 but, for $P_0/P_a = 3.0$ (Fig. 14), the simulation results are higher than the experimental results by up to 100%. We believe that this is due to two factors. First, on the basis of past experience, we expect that the speed of diaphragm rupture will depend on the initial pressure ratio. If this is the case, then this explains why, at
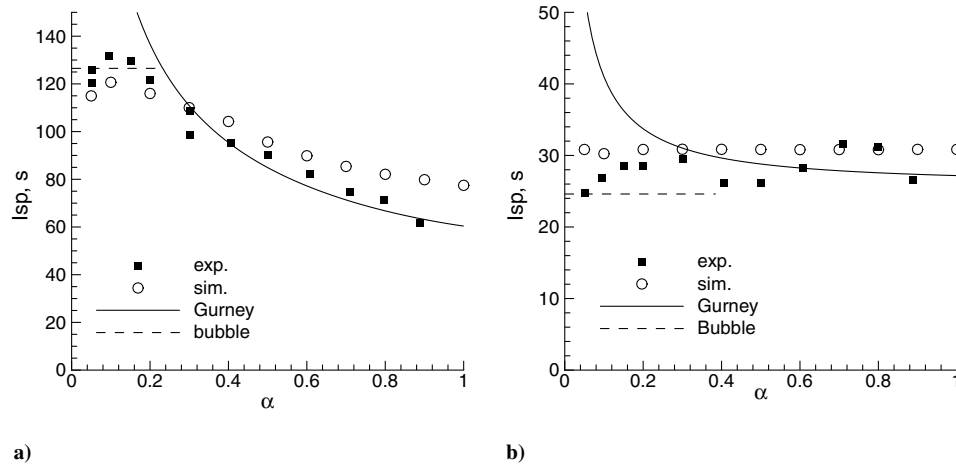
Fig. 12 Specific impulse vs α at $P_0/P_a = 9.2$ for both the simulations (sim.) and experiments (exp.): a) He/air, and b) N_2/air. The Gurney model energy efficiencies were $\eta = 0.178$ for He/air and $\eta = 0.245$ for N_2/air.
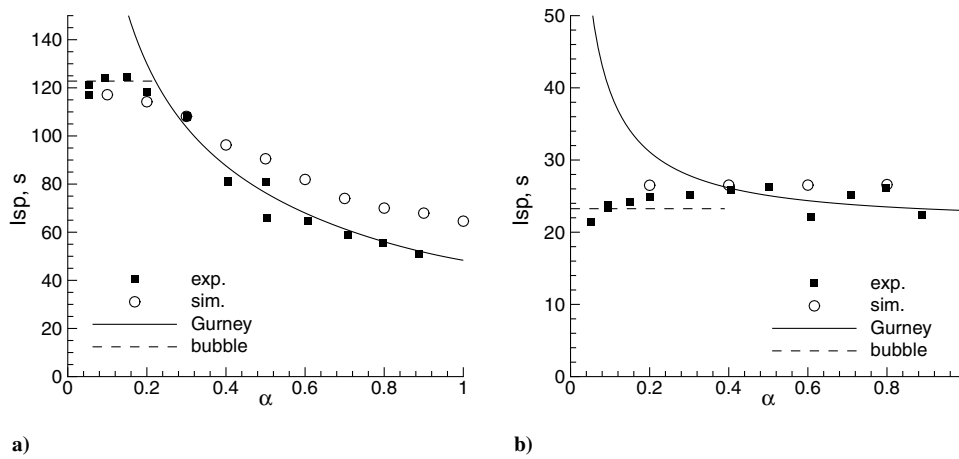

Fig. 13 Specific impulse vs α at $P_0/P_a = 6.0$ for the simulations (sim.) and $P_0/P_a = 6.1$ for the experiments (exp.): a) He/air, and b) N_2/air. The Gurney model energy efficiencies were $\eta = 0.153$ for He/air and $\eta = 0.229$ for N_2/air.
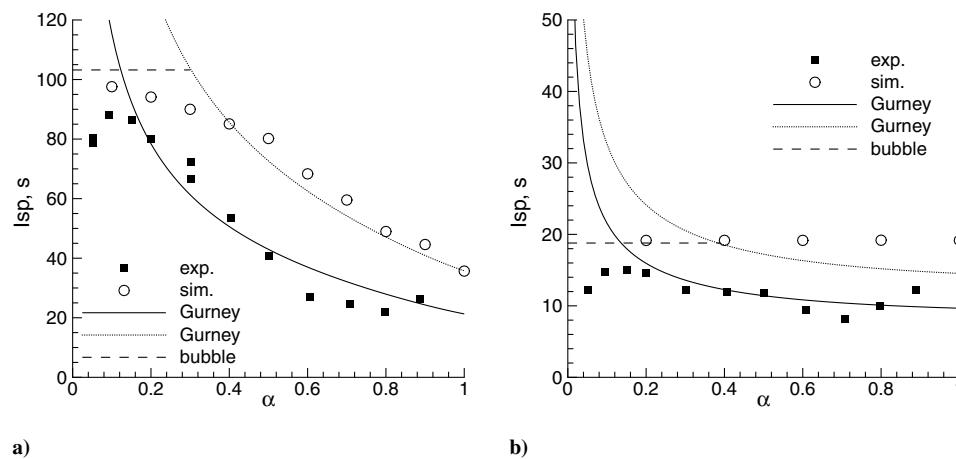

Fig. 14 Specific impulse vs α at $P_0/P_a = 3.0$ for the simulations (sim.) and $P_0/P_a = 3.1$ for the experiments (exp.): a) He/air, and b) N_2/air. The Gurney model energy efficiencies were $\eta = 0.056$ (solid) and $\eta = 0.161$ (dotted) for He/air and $\eta = 0.073$ (solid) and $\eta = 0.168$ (dotted) for N_2/air.

$P_0/P_a = 3.0$, the experimental decay time (Fig. 9) at the thrust wall becomes longer than the computed values (Fig. 8a). Second, if the extension tube becomes longer (α decreases), the ratio of the diaphragm rupture time to the pressure wave propagation time in the tube will become smaller. Therefore, we expect that, at high initial pressure ratios or low fill fractions, the experiments will have the best agreement with the computations.

Effect of Initial Pressure

For both gases (Fig. 15), I_{sp} increases as the pressure ratio increases for a fixed $\alpha = 0.89$. A constant energy efficiency, $\eta = 0.30$, was used for the Gurney model solution. This choice results in reasonable agreement (within 5%) with the simulation when $P_0/P_a > 4.0$, but overpredicts at lower pressure ratios. The increase of the specific impulse with the initial pressure is consistent
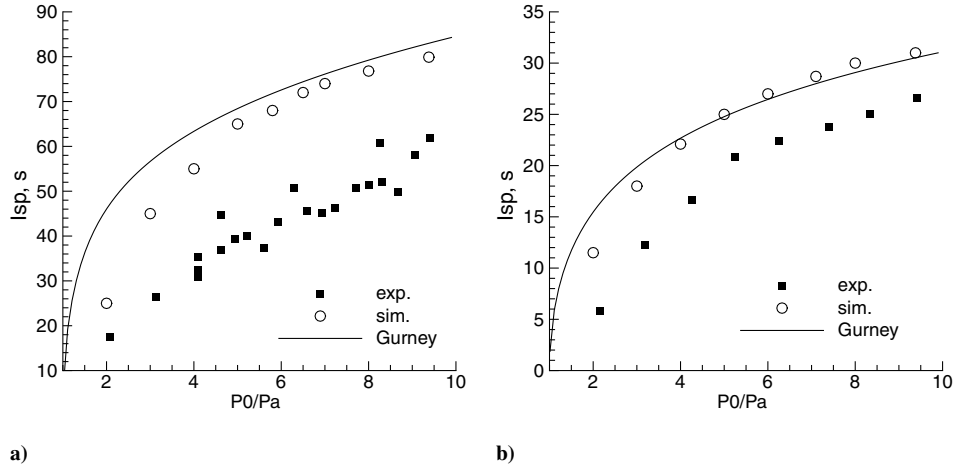
Fig. 15   Specific impulse vs pressure ratio for $\alpha = 0.89$: a) He/air, and b) N_2/air. The Gurney model energy efficiency was $\eta = 30\%$.

with the scaling $I_{sp} \sim \sqrt{e}$ [Eq. (11)] and the dependence of energy on the initial pressure [Eq. (10)]. For the case shown in Fig. 15, the value of α is sufficiently close to 1 that the ratio N/C is small enough to be negligible. The scaling with the square root of energy content is a straightforward consequence of the dimensional analysis and a similar result was obtained previously [16] for pulse detonation tubes.

The simulation results are systematically and substantially higher than the experimental data. For helium, the computational results are larger than the experimental measurements by a factor of 1.5–1.7 when $2.0 < P_0/P_a < 8.0$. For nitrogen, the computational results are larger than the experimental measurements by a factor of ≈ 2.0 when

$P_0/P_a = 2.0$. The difference is smaller at a high pressure ratio; computational results are larger than the experimental measurements by a factor of ≈ 1.2 at $P_0/P_a = 9.2$. As shown in Fig. 14, the difference between the experiments and simulations is large at $\alpha = 0.8$.

Model Comparison

The ratios of $I_{sp}/I_{sp}(\alpha = 1)$ computed from the Gurney model, the Sato model, and the simulation results are shown in Fig. 16 for He/air at three different pressure ratios. Note that this method of comparison eliminates the efficiency factor η dependence from the Gurney
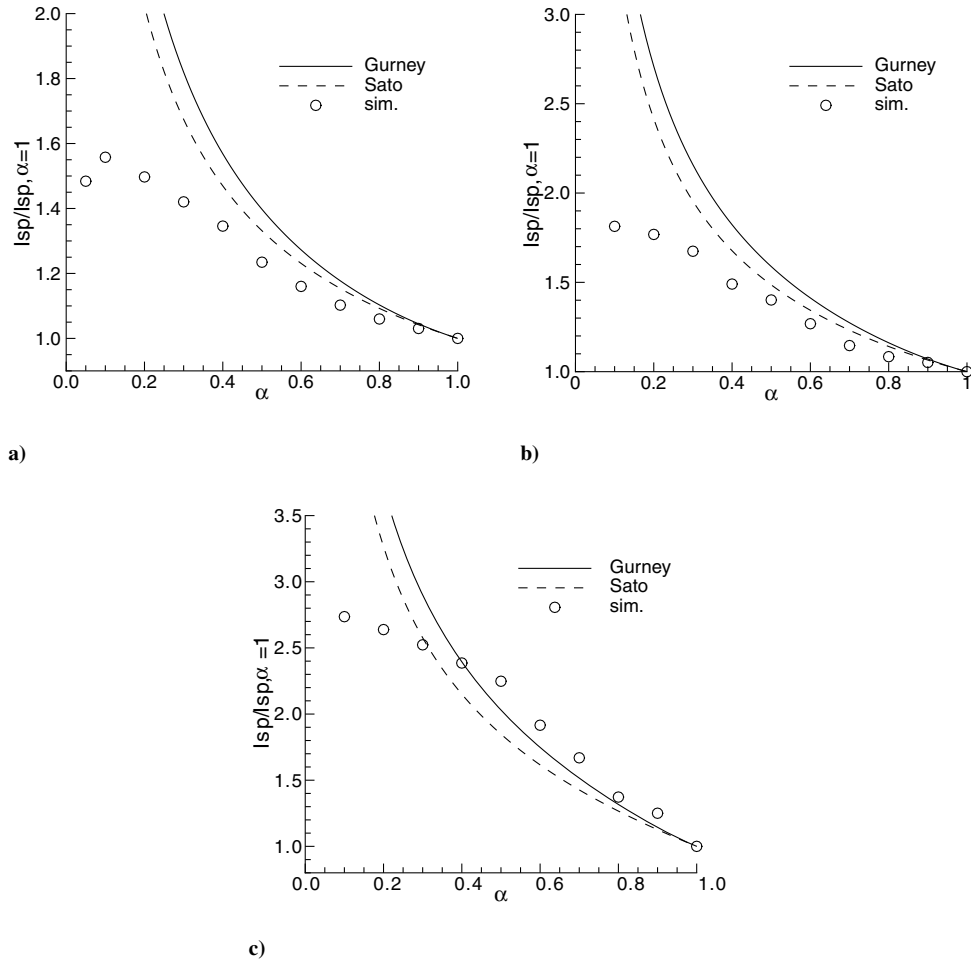

Fig. 16   Normalized specific impulse vs fill fraction of He/air: a) $P_0/P_a = 9.2$, b) $P_0/P_a = 6$, and c) $P_0/P_a = 3$.

Table 5   Energy efficiency η

Gas	P_0/P_a	Simulations	Experiments
He	3.0	0.161	0.056
	6.0	0.197	0.153
	9.2	0.222	0.178
N_2	3.0	0.168	0.073
	6.0	0.229	0.229
	9.2	0.256	0.245

model. Both models show the correct trend for $\alpha > 0.4$ but are completely incorrect for $\alpha < 0.4$, as noted previously. The model predictions at the two highest pressure ratios increasingly overestimate the normalized specific impulse with decreasing values of α. The Gurney model prediction is larger than the Sato model prediction at all fill fractions and initial pressure ratios. The simulation results also show that the maximum ratio of $I_{sp}/I_{sp}(\alpha = 1)$ at $\alpha < 0.2$ is larger for lower pressure ratios, that is, $I_{sp}/I_{sp}(\alpha = 1) \approx 2.7$ for $P_0/P_a = 3$, ≈ 1.8 for $P_0/P_a = 6$, and ≈ 1.5 for $P_0/P_a = 9.2$.

Energy Efficiency

The ideal energy computed in Eq. (10) represents the maximum stored energy in the pressurized gas. In reality, only a fraction η of the stored energy is converted into mechanical energy of the surrounding tube. Cooper and Shepherd [5] computed energy efficiency values for gaseous detonations based on predicted specific impulse values for several mixtures at initial conditions of 100 kPa and 300 K. Their work shows that efficiency values range between 0.124 and 0.305 for gaseous fuel–oxygen–nitrogen mixtures, which are slightly less than the typical propellant efficiency values of 0.2–0.3 and significantly less than the typical efficiency values of 0.6–0.7 for high explosives.

The value of energy efficiency for a pressurized gas release will be different from either gaseous detonation or high explosives and must be determined from comparison of the model with the experimental data. Table 5 gives the estimated values of η that give the best fit to either the simulations or the experimental data for both helium and nitrogen at different pressure ratios. The value of η ranges between 0.056 and 0.256 and is an increasing function of pressure ratio, Fig. 17, for both the experiments and simulations.

Conclusions

We use a shock tube with an open end to study the analog of the partial-fill effect observed in detonation tubes. We carry out experiments and two-dimensional numerical simulations with a range of shock-tube parameters. The specific impulse is measured and computed for two gases, helium and nitrogen, in the driver section with air in the driven section. The initial pressure ratio ranges from $P_0/P_a = 2.0$ to 9.2, and the fill fraction varies from $\alpha = 0.05$ to
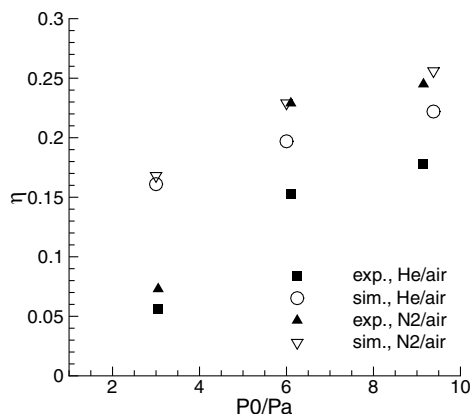
1.0. For both the helium and nitrogen drivers, increasing the pressure ratio with a fixed fill fraction causes the specific impulse to increase. For helium, the specific impulse increases as the fill fraction decreases, reaching a maximum value when $\alpha < 0.2$. For nitrogen, no systematic dependence of specific impulse on fill fraction is observed.

We also compare specific impulse results from numerical simulations, experimental measurements, and analytical models. The numerical simulation results match reasonably well with the experimental measurements for high pressure ratios ($P_0/P_a > 6$) over a large range of fill fractions ($\alpha = 0.05$–0.8), but a systematic difference exists when $\alpha > 0.8$ for all pressure ratios.

When the fill fraction is small ($\alpha < 0.2$), the analytical bubble model predicts a maximum specific impulse. The estimated value shows good agreement (within 5%) with both the numerical computations and experiments for helium at pressure ratios of 6.0 and 9.2, and is 20% higher than the experimental value at a pressure ratio of 3.0. The bubble model slightly underpredicts the impulse for nitrogen at high pressure ratios. When the fill fraction is sufficiently large ($\alpha > 0.2$), the Gurney model predicts the correct trends but the effective energy is much lower than the ideal value and varies with the pressure ratio. Therefore, energy efficiencies must be determined empirically. The computed efficiencies range between 5 and 25% depending on the driver gas and fill fraction. By matching the specific impulse computed from the Gurney model with the experimental data, we find that the energy efficiency is much lower at smaller pressure ratios ($P_0/P_a = 3$: $\eta = 5.6\%$ for helium, $\eta = 7.3\%$ for nitrogen) than at larger pressure ratios ($P_0/P_a = 9.2$: $\eta = 17.8\%$ for helium, $\eta = 24.5\%$ for nitrogen). The Sato and Gurney models yield very similar results and a comparable level of agreement with the experiments and numerical simulations.

The dramatic differences between using nitrogen and helium for the driver show that the partial-fill effect (increase in specific impulse with decreasing fill fraction) is primarily associated with wave processes and is not just due to inertia alone. The differences in density and sound speed between helium and air result in a sharp acoustic impedance discontinuity at the contract surface between the driver and driven section; this traps acoustic waves within the driver and results in the large increase in specific impulse observed in the helium case (see Fig. 11a). No such trapping occurs in the case of nitrogen and, for this reason, the partial-fill effect is not observed in this case (see Fig. 11b). The acoustic analysis of the bubble model captures the difference between helium and nitrogen quantitatively at small fill fractions despite the nonlinear nature of the actual experiments. As the fill fraction approaches 1, the specific impulse decreases with increasing fill fraction. This is in agreement with the Gurney model for helium but not for nitrogen drivers. The disagreement of the Gurney and Sato empirical models with regard to the nitrogen case indicates that energy conservation methods and mass ratios are insufficient to explain the partial-fill effect, although these models show the correct trends for the helium case for values of $\alpha > 0.2$. As the results for nitrogen show, the apparent agreement is fortuitous and the gas dynamic effects associated with the difference in sound speed between the driver and driven sections must be included to explain the partial-fill effect.

The present study is not intended to provide quantitative estimates for pulse detonation engine performance. Pulse detonation tubes or engines have significantly greater complexity than a shock tube, and many other aspects such as flow nonuniformity, heat transfer, valve operation, and fuel mixing must be considered to make quantitative performance estimates. We believe that the real value of our study is to give qualitative guidance about what physical processes and parameters are important in modeling the partial-fill effect. Our study shows clearly that wave propagation processes are essential to the realistic evaluation of the partial-fill effect and that models based on mass or energy conservation alone are inadequate.

Fig. 17   Energy efficiency η vs pressure ratio P_0/P_a for both the simulations (sim.) and experiments (exp.) for He/air and N_2/air.

References

[1] Roy, G. D., Frolov, S. M., Borisov, A. A., and Netzer, D. W., "Pulse Detonation Propulsion: Challenges, Current Status, and Future Perspective," *Progress in Energy and Combustion Science*, Vol. 30, No. 6, 2004, pp. 545–672.
doi:10.1016/j.pecs.2004.05.001

[2] Zhdan, S. A., Mitrofanov, V. V., and Sychev, A. I., "Reactive Impulse from the Explosion of a Gas Mixture in a Semi-infinite Space," *Combustion, Explosion and Shock Waves*, Vol. 30, No. 5, 1994, pp. 657–663.
doi:10.1007/BF00755833

[3] Zitoun, R., and Desbordes, D., "Propulsive Performances of Pulsed Detonations," *Combustion Science and Technology*, Vol. 144, No. 1, 1999, pp. 93–114.
doi:10.1080/00102209908924199

[4] Falempin, F., Bouchaud, D., Forrat, B., Desbordes, D., and Daniau, E., "Pulsed Detonation Engine Possible Application to Low Cost Tactical Missile and to Space Launcher," AIAA Paper 2001-3815, 2001.

[5] Cooper, M., and Shepherd, J. E., "The Effect of Nozzles and Extensions on Detonation Tube Performance," AIAA Paper 02-3628, 2002.

[6] Cooper, M. A., "Impulse Generation by Detonation Tubes," Ph.D. Thesis, California Institute of Technology, Pasadena, CA, May 2004.

[7] Cooper, M., Shepherd, J. E., and Schauer, F., "Impulse Correlation for Partially-Filled Tubes," *Journal of Propulsion and Power*, Vol. 20, No. 5, 2004, pp. 947–950.
doi:10.2514/1.4997

[8] Li, C., and Kailasanath, K., "Performance Analysis of Pulse Detonation Engines with Partial Fuel Filling," *Journal of Propulsion and Power*, Vol. 19 No. 5, 2003, pp. 908–916.

[9] Kasahara, J., Arai, T., and Matsuo, A., "Experimental Analysis of Pulse Detonation Engine Performance by Pressure and Momentum Measurements," AIAA Paper 03-0893, 2003.

[10] Kasahara, J., Tanahashi, Y., Hirano, M., Numata, T., Matsuo, A., and Endo, T., "Experimental Investigation of Momentum and Heat Transfer in Pulse Detonation Rockets," AIAA Paper 04-0869, 2004.

[11] Sato, S., Matsuo, A., Endo, T., and Kasahara, J., "Numerical Studies on Specific Impulse of Partially Filled Pulse Detonation Rocket Engines," *Journal of Propulsion and Power*, Vol. 22, No. 1, 2006, pp. 64–70.
doi:10.2514/1.9514

[12] Endo, T., Yatsufusa, T., Taki, S., Matsuo, A., Inaba, K., and Kasahara, J., "Homogeneous-Dilution Model of Partially-Fueled Simplified Pulse Detonation Engines," *Journal of Propulsion and Power*, Vol. 23, No. 5, 2007, pp. 1033–1041.
doi:10.2514/1.21223

[13] Kasahara, J., Tanahashi, Y., Numata, T., Matsuo, A., and Endo, T., "Experimental Studies on L/D Ratio and Heat Transfer in Pulse Detonations," *19th International Colloquium on the Dynamics of Explosion and Reactive Systems*, ISBN 4-9901744-1-0, 2003; also Paper 65.

[14] Radulescu, M. I., and Hanson, R. K., "Effect of Heat Loss on Pulse-Detonation-Engine Flow Fields and Performance," *Journal of Propulsion and Power*, Vol. 21, No. 2, 2005, pp 274–285.
doi:10.2514/1.10286

[15] Thompson, P. A., *Compressible Fluid Dynamics*, McGraw-Hill, New York, 1972.

[16] Wintenberger, E., Austin, J., Cooper, M., Jackson, S., and Shepherd, J. E., "An Analytical Model for the Impulse of a Single-Cycle Pulse Detonation Engine," *Journal of Propulsion and Power*, Vol. 19, No. 1, 2003, pp. 22–38.

[17] Browne, S., Ziegler, J., and Shepherd, J. E., "Numerical Solution Methods for Shock and Detonation Jump Conditions," California Inst. of Technology, Tech. Rept. FM2006.006, Pasadena, CA, 2004.

[18] Cooper, M., Jackson, S., Austin, J., Wintenberger, E., and Shepherd, J. E., "Direct Experimental Impulse Measurements for Detonations and Deflagrations," *Journal of Propulsion and Power*, Vol. 18, No. 5, 2002, pp. 1033–1041.

[19] Deiterding, R., "High-Resolution Simulation of Detonations with Detailed Chemistry," *Analysis and Numerics for Conservation Laws*, edited by G. Warnecke, Springer–Verlag, Berlin, 2005, pp. 69–91.

[20] Deiterding, R., "A High-Resolution Method for Realistic Detonation Structure Simulation," *Proceedings of the Tenth International Conference on Hyperbolic Problems: Theory, Numerics, Applications*, edited by W. Takahashi, and T. Tanaka, Vol. 1, Yokohama Publishers, Yokohama, Japan, 2004, pp. 343–350.

[21] Gurney, R. W., "The Initial Velocities of Fragments from Bombs, Shells, and Grenades," Army Ballistic Research Laboratory, Tech. Rept. BRL 405, 1943.

[22] Kennedy, J. E., "The Gurney Model of Explosive Output for Driving Metal," *Explosive Effects and Applications*, edited by J. A. Zuker, and W. P. Walters, Springer–Verlag, New York, 1998, pp. 221–257, Chap. 7.

C. Kaplan
Associate Editor